Slice Sampling Reparameterization Gradients

David M. Zoltowski ZOLTOWSKI@PRINCETON.EDU
Diana Cai DCAI@CS.PRINCETON.EDU
Ryan P. Adams RPA@PRINCETON.EDU
Princeton University

Abstract

Slice sampling is a Markov chain Monte Carlo algorithm for simulating samples from probability distributions, with the convenient property that it is rejection-free. When the slice endpoints are known, the sampling path is a deterministic function of noise variables since there are no accept-reject steps like those in Metropolis-Hastings algorithms. Here we describe how to differentiate the slice sampling path to compute *slice sampling reparameterization gradients*. Since slice sampling does not require a normalizing constant, this allows for computing reparameterization gradients of samples from potentially complicated multivariate distributions. We apply the method in synthetic examples and to fit a variational autoencoder with a conditional energy-based model approximate posterior.

1. Introduction

Probabilistic objectives that take the form of an expectation of a function with respect to a base density $p_\theta(x)$, i.e.,

$$\mathcal{L}(\theta) = \mathbb{E}_{p_\theta(x)}[\ell(x)], \tag{1}$$

are common in machine learning. Typically, this expectation cannot be computed in closed form, so optimizing this objective with respect to the distributional parameters θ requires stochastic estimates of the gradient of the expectation. Stochastic gradients estimators arise in a number of machine learning applications, including optimizing the evidence lower bound (ELBO) in variational inference (Blei et al., 2017), forming the policy gradient in reinforcement learning (Sutton et al., 1998), and optimizing the probability of improvement in experimental design (Wilson et al., 2018).

Two popular classes of gradient estimators are score function gradients and reparameterization (or pathwise) gradients; see Mohamed et al. (2019) for a review. Reparameterization gradients apply when samples from $p_\theta(x)$ can be generated by a deterministic transformation f_θ of samples from a base distribution $p(\epsilon)$. That is, if $\tilde{\epsilon} \sim p(\epsilon)$ then $\tilde{x} = f_\theta(\tilde{\epsilon}) \sim p_\theta(x)$. Applying this transformation, the gradient of the objective with respect to θ can then be expressed as an expectation with respect to a distribution that does not depend on θ: under mild regularity conditions,

$$\nabla_\theta \mathcal{L}(\theta) = \nabla_\theta \mathbb{E}_{p(\epsilon)}[\ell(f_\theta(\epsilon))] = \mathbb{E}_{p(\epsilon)}[\nabla_\theta \ell(f_\theta(\epsilon))]. \tag{2}$$

Monte Carlo estimates of the gradient are then computed using samples from $p(\epsilon)$.

There are many examples of reparameterization gradients (Appendix A), but they typically are restricted to distributions with tractable normalization constants. Recent work has extended reparameterization gradients to unnormalized probability distributions using reparameterized Markov chain Monte Carlo (MCMC) algorithms, including Gibbs samplers with reparameterizable Gibbs sampling steps (Vahdat et al., 2020) and dynamics-based MCMC samplers without accept/reject steps (e.g., Salimans et al. 2015; Dai et al. 2019). However, not all Gibbs sampling steps are reparameterizable using current methods, and dynamics-based MCMC samplers without accept/reject steps are approximate samplers. Unfortunately, the sampling paths of MCMC algorithms with accept/reject steps are not deterministic and differentiable, precluding the use of reparameterization gradients. Instead, score function gradients or specialized methods for discrete variables or accept/reject steps (Naesseth et al., 2016) would need to be used to estimate gradients from such methods.

In this work, we develop reparameterization gradients for samples generated from slice sampling. Slice sampling (Neal, 2003) is an MCMC algorithm for simulating samples from distributions $p_\theta(x) = \pi_\theta(x)/Z(\theta)$ where the normalizing constant $Z(\theta)$ may be unknown. It is often an appealing alternative to the Metropolis-Hastings algorithm, as slice sampling does not require an accept/reject step or sensitive tuning parameters. The lack of an accept/reject step means that, for a fixed pseudo-random sequence, the realized slice sampling Markov chain is differentiable with respect to the parameters θ. Slice sampling reparameterization gradients apply to complicated multivariate distributions such as energy-based models (EBMs, LeCun et al., 2006). However, the generated samples are correlated and the gradient estimates are biased because we simulate from a finite Markov chain. In our experiments, we demonstrate the efficacy of slice sampling reparameterization gradients and use them to fit a conditional EBM as an approximate posterior in a variational autoencoder.

2. Slice sampling reparameterization gradients

Consider a distribution with density $p(\boldsymbol{x}) = \frac{1}{Z}\pi(\boldsymbol{x})$ where the normalizing constant may not be known. In slice sampling, samples are simulated from the distribution by uniformly sampling under the surface of the density (Neal, 2003), typically via two steps. Starting from an initial point $\boldsymbol{x}_n$, a height y_{n+1} is sampled uniformly beneath the density at $\boldsymbol{x}_n$ such that $y_{n+1} \sim \mathcal{U}(0, \pi(\boldsymbol{x}_n))$. The height y_{n+1} defines a slice through the surface of the probability density given by $S = \{\boldsymbol{x} : y_{n+1} < \pi(\boldsymbol{x})\}$. The next point $\boldsymbol{x}_{n+1}$ is then sampled uniformly from the set S. We use *random-direction slice sampling* to sample from the set S (MacKay, 2002, Chapter 29.7). A random direction $\boldsymbol{d}$ is generated from a uniform distribution over directions, and the direction defines a line segment through the slice with endpoints $\boldsymbol{x}^-$ and $\boldsymbol{x}^+$. Finally, a value $\boldsymbol{x}_{n+1}$ is sampled uniformly between the endpoints. The most common procedure for finding the endpoints, as proposed by Neal (2003), is to use a reversible "stepping-out" procedure followed by "interval shrinking" to determine $\boldsymbol{x}_{n+1}$; we do not use these procedures and instead perform a direct search for the slice boundaries.

2.1. Random-direction slice sampling with numerical slice endpoints

Here we describe the steps of random-direction slice sampling in more detail. We start from a point $\boldsymbol{x}_n \in \mathbb{R}^d$ and a continuous, unnormalized density with parameters θ, $\pi_\theta(\boldsymbol{x})$. We sample three random quantities: two uniform random numbers $u_1, u_2 \in [0, 1]$ and a uniform random unit vector $\boldsymbol{d}$. The value u_1 determines the height of the slice $u_1\pi_\theta(\boldsymbol{x}_n)$. The direction $\boldsymbol{d}$ defines a line through the slice. This line intersects with the density at

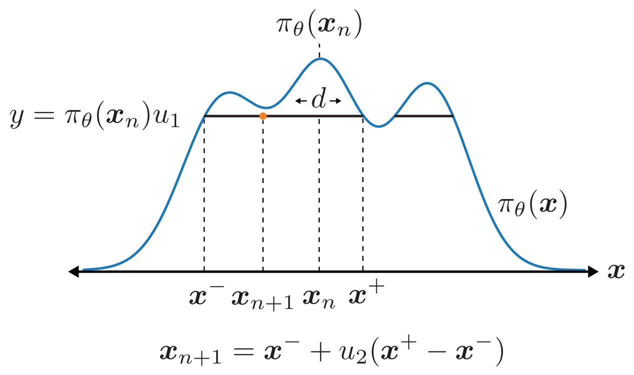
$\pi_\theta(\boldsymbol{x}_n)$
$y = \pi_\theta(\boldsymbol{x}_n)u_1$
d
$\pi_\theta(\boldsymbol{x})$
$\boldsymbol{x}$
$\boldsymbol{x}^-$ $\boldsymbol{x}_{n+1}$ $\boldsymbol{x}_n$ $\boldsymbol{x}^+$
$\boldsymbol{x}_{n+1} = \boldsymbol{x}^- + u_2(\boldsymbol{x}^+ - \boldsymbol{x}^-)$

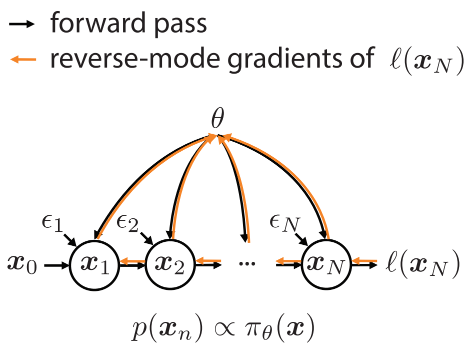
forward pass
reverse-mode gradients of $\ell(\boldsymbol{x}_N)$
θ
ϵ_1 ϵ_2 ϵ_N
$\boldsymbol{x}_0$ $\boldsymbol{x}_1$ $\boldsymbol{x}_2$ ... $\boldsymbol{x}_N$ $\ell(\boldsymbol{x}_N)$
$p(\boldsymbol{x}_n) \propto \pi_\theta(\boldsymbol{x})$

Figure 1: Slice sampling. *Left*: Visualization of one step of a 1D slice sampler. *Right*: Reparameterized slice sampling computational graph with reverse mode gradients shown for a loss computed on the final sample $\boldsymbol{x}_N$.

points where $\pi_\theta(\boldsymbol{x}_n + \alpha\boldsymbol{d}) = u_1\pi_\theta(\boldsymbol{x}_n)$ for scalar values α. These correspond to a set

$$\mathcal{A} = \{\alpha : \pi_\theta(\boldsymbol{x}_n + \alpha\boldsymbol{d}) = u_1\pi_\theta(\boldsymbol{x}_n)\}\,. \tag{3}$$

Two specific members of this set, $\alpha^+ = \min_{\alpha>0}\mathcal{A}$ and $\alpha^- = \max_{\alpha<0}\mathcal{A}$, define the slice endpoints $\boldsymbol{x}^- = \boldsymbol{x}_n + \alpha^-\boldsymbol{d}$ and $\boldsymbol{x}^+ = \boldsymbol{x}_n + \alpha^+\boldsymbol{d}$. These are the closest locations on the slice in the positive and negative direction where $\pi_\theta(\boldsymbol{x}_n + \alpha\boldsymbol{d}) = u_1\pi_\theta(\boldsymbol{x}_n)$. We identify α^+ and α^- using numerical root finding (Appendix E). Then, the next sample $\boldsymbol{x}_{n+1}$ is sampled uniformly between the endpoints $\boldsymbol{x}^-$ and $\boldsymbol{x}^+$ such that

$$\boldsymbol{x}_{n+1} = \boldsymbol{x}^- + u_2(\boldsymbol{x}^+ - \boldsymbol{x}^-) = \boldsymbol{x}_n + u_2\alpha^+\boldsymbol{d} + (1-u_2)\alpha^-\boldsymbol{d}\,. \tag{4}$$

We can view α^- and α^+ as implicit functions of $\boldsymbol{x}_n$, $\boldsymbol{d}$, u_1, and θ, denoted $\alpha^+(\boldsymbol{x}_n, \boldsymbol{d}, u_1, \theta)$, and $\alpha^-(\boldsymbol{x}_n, \boldsymbol{d}, u_1, \theta)$. Via equation (4), the location $\boldsymbol{x}_{n+1}$ is then a deterministic function of $\boldsymbol{x}_n$, θ, the random variables u_1, u_2, and $\boldsymbol{d}$:

$$\boldsymbol{x}_{n+1} = \boldsymbol{x}_n + u_2\,\alpha^+(\boldsymbol{x}_n, \boldsymbol{d}, u_1, \theta)\,\boldsymbol{d} + (1-u_2)\,\alpha^-(\boldsymbol{x}_n, \boldsymbol{d}, u_1, \theta)\,\boldsymbol{d}\,. \tag{5}$$

In Figure 1 and later sections, we use ϵ to refer to u_1, u_2, and $\boldsymbol{d}$ such that $\boldsymbol{x}_{n+1} = s(\boldsymbol{x}_n, \theta, \epsilon)$.

2.2. Reverse mode gradients

The slice sampling procedure generates samples $\boldsymbol{x}_{1:N}$. After generating the samples, we evaluate the objective function and use reverse mode automatic differentiation (AD) to compute gradients (Griewank and Walther, 2008, Section 3.2; Baydin et al., 2017). Here we derive the reverse mode gradients. Our derivation uses implicit differentiation to efficiently compute gradients of the slice endpoints, avoiding the need to compute gradients through the numerical root finding algorithm. Each sample $\boldsymbol{x}_{n+1}$ depends on the previous samples $\boldsymbol{x}_{1:n}$ and the parameters θ, as shown by the computational graph (Figure 1). To compute gradients with respect to the parameters (and initial condition) we therefore require the

Jacobian of $\boldsymbol{x}_{n+1}$ with respect to $\boldsymbol{x}_n$ and with respect to θ. We denote these $\mathcal{J}_{\boldsymbol{x}_n}(\boldsymbol{x}_{n+1})$ and $\mathcal{J}_\theta(\boldsymbol{x}_{n+1})$. Using equation (4) for $\boldsymbol{x}_n$, these Jacobians can be computed indirectly via adjoints

$$\mathcal{J}_{\boldsymbol{x}_n}\left(\boldsymbol{x}_n + \boldsymbol{d}u_2\alpha^+ + \boldsymbol{d}(1-u_2)\alpha^-\right) = \boldsymbol{I} + u_2\boldsymbol{d}\nabla_{\boldsymbol{x}_n}[\alpha^+]^\mathsf{T} + (1-u_2)\boldsymbol{d}\nabla_{\boldsymbol{x}_n}[\alpha^-]^\mathsf{T} \tag{6}$$

$$\mathcal{J}_\theta\left(\boldsymbol{x}_n + \boldsymbol{d}u_2\alpha^+ + \boldsymbol{d}(1-u_2)\alpha^-\right) = u_2\boldsymbol{d}\nabla_\theta[\alpha^+]^\mathsf{T} + (1-u_2)\boldsymbol{d}\nabla_\theta[\alpha^-]^\mathsf{T}. \tag{7}$$

We use implicit differentiation to compute $\nabla_{\boldsymbol{x}_n}[\alpha^{+,-}]$. The values α are solutions to

$$f(\boldsymbol{x}_n, \boldsymbol{d}, \alpha, \theta) = \ln \pi_\theta(\boldsymbol{x}_n + \alpha\boldsymbol{d}) - \ln u_1 - \ln \pi_\theta(\boldsymbol{x}_n) = 0. \tag{8}$$

Applying implicit differentiation (Griewank and Walther, 2008, Chap. 15) we get:

$$\nabla_{\boldsymbol{x}_n}\alpha = -\frac{\nabla_{\boldsymbol{x}_n} f}{\partial f/\partial\alpha} = -\frac{\nabla_{\boldsymbol{x}_n}\ln\pi_\theta(\boldsymbol{x}_n+\alpha\boldsymbol{d}) - \nabla_{\boldsymbol{x}_n}\ln\pi_\theta(\boldsymbol{x}_n)}{\boldsymbol{d}^\mathsf{T}\nabla_{\boldsymbol{x}_n}\ln\pi_\theta(\boldsymbol{x}_n+\alpha\boldsymbol{d})} \tag{9}$$

$$\nabla_\theta\alpha = -\frac{\nabla_\theta f}{\partial f/\partial\alpha} = -\frac{\nabla_\theta\ln\pi_\theta(\boldsymbol{x}_n+\alpha\boldsymbol{d}) - \nabla_\theta\ln\pi_\theta(\boldsymbol{x}_n)}{\boldsymbol{d}^\mathsf{T}\nabla_{\boldsymbol{x}_n}\ln\pi_\theta(\boldsymbol{x}_n+\alpha\boldsymbol{d})}. \tag{10}$$

Let the loss be a sum over the samples $\boldsymbol{x}_n$ such that $L(\theta) = \frac{1}{N}\sum_{n=1}^N \ell_n(\boldsymbol{x}_n)$. The gradient of the loss with respect to θ is

$$\nabla_\theta L = \sum_{n=1}^N [\mathcal{J}_\theta(\boldsymbol{x}_n)]^\mathsf{T}\nabla_{\boldsymbol{x}_n} L. \tag{11}$$

The gradient $\nabla_\theta L$ depends on the gradients of the loss with respect to each sample, $\nabla_{\boldsymbol{x}_n} L$. For the final sample $\boldsymbol{x}_N$ this gradient is simply $\nabla_{\boldsymbol{x}_N} L = \frac{1}{N}\nabla_{\boldsymbol{x}_N}\ell_n(\boldsymbol{x}_N)$. For earlier samples $\boldsymbol{x}_n$ where $n = 1, ..., N-1$, the loss gradients need to be propagated backwards via

$$\nabla_{\boldsymbol{x}_n} L = \frac{1}{N}\nabla_{\boldsymbol{x}_n}\ell_n(\boldsymbol{x}_n) + [\mathcal{J}_{\boldsymbol{x}_n}(\boldsymbol{x}_{n+1})]^\mathsf{T}\nabla_{\boldsymbol{x}_{n+1}} L. \tag{12}$$

After computing $\{\nabla_{\boldsymbol{x}_1} L, ...\nabla_{\boldsymbol{x}_N} L\}$, the gradient is given by equation (11). Critically, we compute $\nabla_\theta L$ without ever fully representing either of the Jacobians by using vector-Jacobian products (Appendix B). We implemented the forward sampling and reverse mode AD in JAX (Bradbury et al., 2018).

2.3. Gradient of the ELBO

We use the reparameterized slice sampler to optimize the ELBO in variational inference with an unnormalized density $q_\phi(\boldsymbol{z}) = \frac{1}{Z(\phi)}e^{f_\phi(\boldsymbol{z})}$ with parameters ϕ as the approximate posterior. The reparameterized ELBO is

$$\mathcal{L}(\theta,\phi) = \mathbb{E}_{q_\phi(\boldsymbol{z})}[\log p_\theta(\boldsymbol{x},\boldsymbol{z}) - \log q_\phi(\boldsymbol{z})] = \mathbb{E}_{p(\epsilon)}[\log p_\theta(\boldsymbol{x},\boldsymbol{z}(\phi,\epsilon)) - \log q_\phi(\boldsymbol{z}(\phi,\epsilon))], \tag{13}$$

where $\boldsymbol{z}(\phi,\epsilon)$ is a sample generated from the reparameterized slice sampler with unnormalized density $f_\phi(\boldsymbol{z})$ and base random variables ϵ. Estimating the gradient appears to require the gradient of the normalizing constant $Z(\phi)$. However, applying the total derivative (Roeder et al., 2017) yields a path derivative Monte Carlo estimator of the gradient for a sample ϵ that does not require the normalizing constant:

$$\hat{\nabla}_{\mathrm{PD}}(\epsilon,\phi) = \nabla_{\boldsymbol{z}}[\log p_\theta(\boldsymbol{x},\boldsymbol{z}(\phi,\epsilon)) - f_\phi(\boldsymbol{z}(\phi,\epsilon))]\nabla_\phi\boldsymbol{z}(\phi,\epsilon). \tag{14}$$

See Appendix C for a full derivation. This estimator has favorable performance, and has zero variance when $p_\theta(\boldsymbol{z} \mid \boldsymbol{x}) = q_\phi(\boldsymbol{z} \mid \boldsymbol{x})$ (Roeder et al., 2017).

3. Experiments

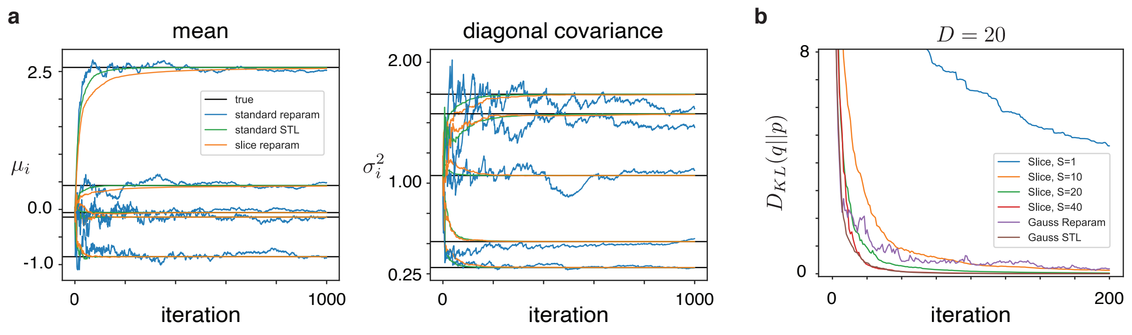

Figure 2: Matching an independent Gaussian. (**a**) Mean and diagonal covariance elements as a function of iteration. (**b**) Loss as a function of iteration for slice sampling reparameterization gradients computed using different chain lengths S.

Matching a target independent Gaussian First, we optimize $\min_\phi D_{KL}(q_\phi||p)$ where q and p are both multivariate Gaussians with diagonal covariances. First, we show that the parameters ϕ optimized with slice sampling reparameterization gradients converge to the target values for a low-dimensional example with $D = 5$ (Figure 2). Next, for $D = 20$ we compare performance with different chain lengths S. The gradient is computed by backpropagating the loss of the final sample. As S approaches D, slice sampling reparameterization gradients perform competitively with standard reparameterization gradients.

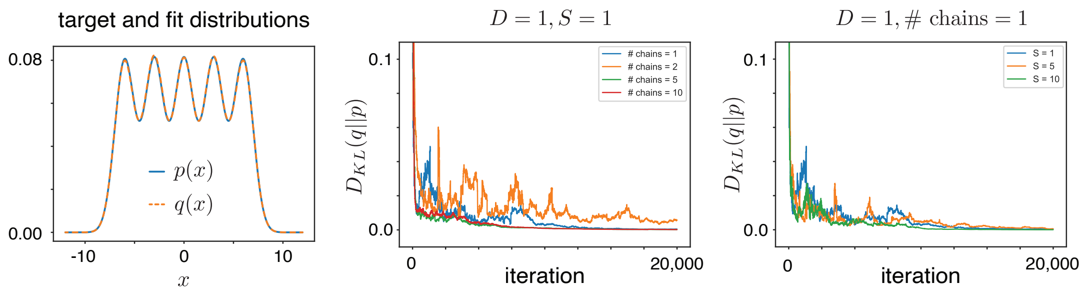

Figure 3: Fitting a mixture of Gaussians with variable numbers of samples and chains.

Matching a target mixture of Gaussians Next, we minimize $D_{KL}(q_\phi||p)$ with respect to ϕ where q and p are 1D mixtures of Gaussians (Figure 3). We estimated gradients using N independent chains each of length S samples. While performance is reasonable with $S = 1$ and $N = 1$, increasing the number of independent chains and the number of samples improved performance. In conclusion, for multimodal distributions it may be advantageous to run multiple independent chains or increase the number of samples beyond the dimensionality of the space.

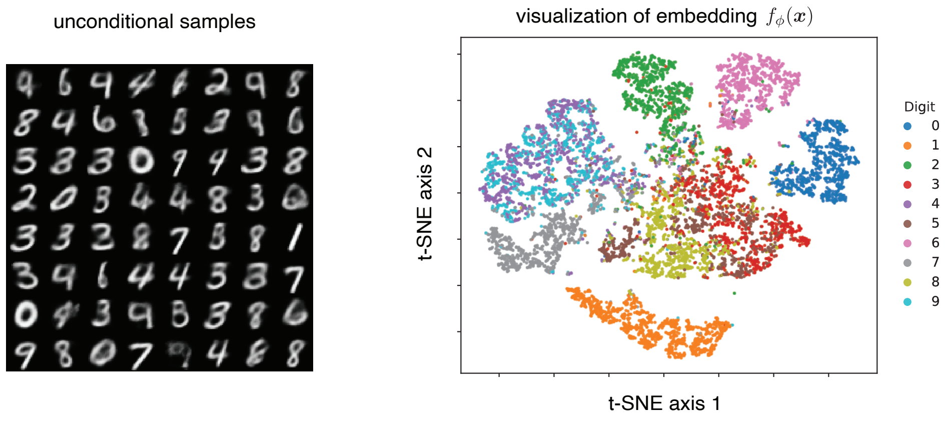

Figure 4: Unconditional samples (*left*) and embedding visualization (*right*) of a VAE fit to MNIST with an EBM approximate posterior.

VAE with conditional EBM approximate posterior We used slice sampling reparameterization gradients to fit a variational autoencoder (VAE) (Kingma and Welling, 2013; Rezende et al., 2014) with a conditional EBM as the approximate posterior:

$$q(\boldsymbol{z} \mid \boldsymbol{x}) = \frac{1}{Z(\theta, \boldsymbol{x})} \exp\{f_\phi(\boldsymbol{x})^\top g_\phi(\boldsymbol{z}) + \log p_0(\boldsymbol{z})\}. \tag{15}$$

The observations are $\boldsymbol{x}$, the latent variables are $\boldsymbol{z} \in \mathbb{R}^D$, and $\log p_0(\boldsymbol{z})$ is a prior. The functions $f_\phi(\boldsymbol{x})$ and $g_\phi(\boldsymbol{z})$ map to vectors with an embedding dimensionality D_e. This differs from the standard VAE in that the encoder f does not map to the mean of the latent space, but rather a separate embedding that is nonlinearly combined by $g(\boldsymbol{z})$ to give the energy. The form of the conditional EBM has been studied previously in Khemakhem et al. (2019, 2020). We fit the VAE to MNIST data with a Bernoulli log likelihood and with $D = 20$ and $D_e = 50$. The gradients were estimated over mini batches of size 64 with one MCMC chain of $S = 100$ samples for each image. We ran the optimization for 200 epochs. Unconditional samples from the generative model look reasonable (Figure 4). We visualized the embedding of held out test images by the function f using t-SNE (Maaten and Hinton, 2008). Interestingly, we see clusters in the embedding space corresponding to digits, with some overlap for similar digits.

4. Discussion

We presented slice sampling reparameterization gradients that apply to multivariate distributions without a normalizing constant, and demonstrated the method with synthetic examples and by fitting a conditional EBM approximate posterior. In future work we will extend our experimental evaluation of the method, investigate methods to improve VAE training, and explore additional applications of the method.

Acknowledgments

We thank Dougal Maclaurin for valuable discussions. This work was partially funded by NSF IIS-2007278. D. Zoltowski was supported in part by NIH grant T32MH065214. D. Cai was supported in part by a Google Ph.D. Fellowship in Machine Learning.

References

Atılım Günes Baydin, Barak A Pearlmutter, Alexey Andreyevich Radul, and Jeffrey Mark Siskind. Automatic differentiation in machine learning: a survey. *The Journal of Machine Learning Research*, 18(1):5595–5637, 2017.

David M Blei, Alp Kucukelbir, and Jon D McAuliffe. Variational inference: A review for statisticians. *Journal of the American Statistical Association*, 112(518):859–877, 2017.

Samuel R Bowman, Luke Vilnis, Oriol Vinyals, Andrew M Dai, Rafal Jozefowicz, and Samy Bengio. Generating sentences from a continuous space. *arXiv preprint arXiv:1511.06349*, 2015.

James Bradbury, Roy Frostig, Peter Hawkins, Matthew James Johnson, Chris Leary, Dougal Maclaurin, and Skye Wanderman-Milne. JAX: composable transformations of Python+NumPy programs, 2018. URL http://github.com/google/jax.

Bo Dai, Zhen Liu, Hanjun Dai, Niao He, Arthur Gretton, Le Song, and Dale Schuurmans. Exponential family estimation via adversarial dynamics embedding. In *Advances in Neural Information Processing Systems*, pages 10979–10990, 2019.

Adji Bousso Dieng, Dustin Tran, Rajesh Ranganath, John Paisley, and David Blei. Variational inference via χ upper bound minimization. In *Advances in Neural Information Processing Systems*, pages 2732–2741, 2017.

Mikhail Figurnov, Shakir Mohamed, and Andriy Mnih. Implicit reparameterization gradients. In *Advances in Neural Information Processing Systems*, pages 441–452, 2018.

Ian Goodfellow, Jean Pouget-Abadie, Mehdi Mirza, Bing Xu, David Warde-Farley, Sherjil Ozair, Aaron Courville, and Yoshua Bengio. Generative adversarial nets. *Advances in neural information processing systems*, 27:2672–2680, 2014.

Will Grathwohl, Kuan-Chieh Wang, Jörn-Henrik Jacobsen, David Duvenaud, Mohammad Norouzi, and Kevin Swersky. Your classifier is secretly an energy based model and you should treat it like one. *arXiv preprint arXiv:1912.03263*, 2019.

Andreas Griewank and Andrea Walther. *Evaluating derivatives: principles and techniques of algorithmic differentiation*. SIAM, 2008.

Matthew D Hoffman and Matthew J Johnson. Elbo surgery: yet another way to carve up the variational evidence lower bound. In *Workshop in Advances in Approximate Bayesian Inference, NIPS*, volume 1, page 2, 2016.

Ilyes Khemakhem, Diederik P Kingma, and Aapo Hyvärinen. Variational autoencoders and nonlinear ICA: A unifying framework. *arXiv preprint arXiv:1907.04809*, 2019.

Ilyes Khemakhem, Ricardo Pio Monti, Diederik P Kingma, and Aapo Hyvärinen. ICE-BeeM: Identifiable conditional energy-based deep models. *arXiv preprint arXiv:2002.11537*, 2020.

Diederik P Kingma and Max Welling. Auto-encoding variational Bayes. *arXiv preprint arXiv:1312.6114*, 2013.

Yann LeCun, Sumit Chopra, Raia Hadsell, M Ranzato, and F Huang. A tutorial on energy-based learning. *Predicting Structured Data*, 1(0), 2006.

Laurens van der Maaten and Geoffrey Hinton. Visualizing data using t-SNE. *Journal of Machine Learning Research*, 9(Nov):2579–2605, 2008.

David J. C. MacKay. *Information Theory, Inference & Learning Algorithms.* Cambridge University Press, USA, 2002. ISBN 0521642981.

Shakir Mohamed, Mihaela Rosca, Michael Figurnov, and Andriy Mnih. Monte Carlo gradient estimation in machine learning. *arXiv preprint arXiv:1906.10652*, 2019.

Christian A Naesseth, Francisco JR Ruiz, Scott W Linderman, and David M Blei. Reparameterization gradients through acceptance-rejection sampling algorithms. *arXiv preprint arXiv:1610.05683*, 2016.

Radford M Neal. Slice sampling. *Annals of statistics*, pages 705–741, 2003.

Erik Nijkamp, Mitch Hill, Tian Han, Song-Chun Zhu, and Ying Nian Wu. On the anatomy of MCMC-based maximum likelihood learning of energy-based models. *arXiv preprint arXiv:1903.12370*, 2019a.

Erik Nijkamp, Mitch Hill, Song-Chun Zhu, and Ying Nian Wu. Learning non-convergent non-persistent short-run MCMC toward energy-based model. In *Advances in Neural Information Processing Systems*, pages 5233–5243, 2019b.

Tom Rainforth, Adam R Kosiorek, Tuan Anh Le, Chris J Maddison, Maximilian Igl, Frank Wood, and Yee Whye Teh. Tighter variational bounds are not necessarily better. In *ICML*, 2018.

Danilo Jimenez Rezende, Shakir Mohamed, and Daan Wierstra. Stochastic backpropagation and approximate inference in deep generative models. *arXiv preprint arXiv:1401.4082*, 2014.

Geoffrey Roeder, Yuhuai Wu, and David K Duvenaud. Sticking the landing: Simple, lower-variance gradient estimators for variational inference. In *Advances in Neural Information Processing Systems*, pages 6925–6934, 2017.

Francisco JR Ruiz, Michalis K Titsias, and David M Blei. The generalized reparameterization gradient. In *Advances in neural information processing systems*, pages 460–468, 2016.

Tim Salimans, Diederik Kingma, and Max Welling. Markov chain Monte Carlo and variational inference: Bridging the gap. In *International Conference on Machine Learning*, pages 1218–1226, 2015.

Richard S Sutton, Andrew G Barto, et al. *Introduction to reinforcement learning*, volume 135. MIT press Cambridge, 1998.

George Tucker, Dieterich Lawson, Shixiang Gu, and Chris J Maddison. Doubly reparameterized gradient estimators for Monte Carlo objectives. In *International Conference on Learning Representations*, 2018.

Arash Vahdat, Evgeny Andriyash, and William G Macready. Undirected graphical models as approximate posteriors. In *International Conference on Machine Learning (ICML)*, 2020.

James Wilson, Frank Hutter, and Marc Deisenroth. Maximizing acquisition functions for Bayesian optimization. In *Advances in Neural Information Processing Systems*, pages 9884–9895, 2018.

Appendix A. Related work

Reparameterization gradients We focus here on continuous distributions, for which many examples of reparameterization gradients exist. "One-liner" reparameterization gradients use a simple function to transform the base distribution into the desired parameterized distribution (Kingma and Welling, 2013; Rezende et al., 2014; Mohamed et al., 2019). Next, the inverse CDF can be used to transform uniform random variables into arbitrary 1D distributions, and gradients can be computed when evaluating and differentiating the inverse CDF are numerically tractable. Additional examples of reparameterization gradients are implicit reparameterization gradients (Figurnov et al., 2018), doubly reparameterized gradients (Tucker et al., 2018), reparameterization of accept/reject sampling (Naesseth et al., 2016), and generalized reparameterization gradients (Ruiz et al., 2016). Other recent work has also described reparameterizing MCMC samplers for gradient estimation.

Generative neural samplers are another approach for simulating reparameterized samples from a complicated distribution, although they are not an MCMC algorithm. In this approach, random variables are passed through a neural network to generate samples from a more complicated distribution. This is the approach taken in the generator of a GAN (Goodfellow et al., 2014). However, this method does not directly apply to generating samples from an unnormalized distribution with a prescribed energy function, since there is not a closed form description of the distribution of the generated samples. Additionally, the parameters of the neural network must be tuned to match the desired distribution through a complicated optimization process. In contrast, the reparameterized slice sampler directly samples from a distribution with a prescribed energy function without the need for an optimization process.

Variational autoencoders Variational autoencoders (VAEs) are a class of deep generative models fit with amortized variational inference (Kingma and Welling, 2013; Rezende et al., 2014). The generative model is

$$\boldsymbol{z} \sim \mathcal{N}(0, I), \quad \boldsymbol{x} \mid \boldsymbol{z} \sim \mathcal{N}(\mu_\theta(\boldsymbol{z}), \sigma_\theta(\boldsymbol{z})) \tag{16}$$

where μ_θ and σ_θ are neural networks with parameters θ. The model has typically been fit using variational inference with an amortized Gaussian approximate posterior $q_\phi(\boldsymbol{z} \mid \boldsymbol{z}) = \mathcal{N}(\mu_\phi(\boldsymbol{x}), \sigma_\phi(\boldsymbol{x}))$ by maximizing the ELBO, although other inference methods and types of approximate posteriors have been studied.

In VAEs, it has been observed that the approximate posterior may collapse to the prior distribution (Bowman et al., 2015; Hoffman and Johnson, 2016). A number of papers have proposed methods to solve this problem and others related to VAE training. One approach is to the alter the generative model. For example, Dieng et al. (2017) showed that adding skip connections to the generative model helps avoid posterior collapse and improves the latent variable representation. We did not investigate if the VAE trained with a conditional EBM approximate posterior improved posterior collapse. However, we did show interesting structure given by the embedding function f. Similar to the encoder network of a standard VAE, which maps to the mean of a multivariate Guassian distributions, this function provides a low-dimensional representation of the input data. It will be interesting to compare the representations of these two approaches in follow up experiments.

Energy-based models Energy-based models are under increasingly active study. Grathwohl et al. (2019) relate classifiers with softmax outputs to EBMs, and propose a method for jointly training a classifier and generative model. Nijkamp et al. (2019b,a) describe using SGLD for learning deep EBMs for image data, and provide informative analysis on short run vs. long run MCMC for training EBMs. We expect that reparamterization gradient methods for unnoramlized distributions will enable additional use cases for EBMs.

Appendix B. Efficient computation

Importantly, we can compute $\nabla_\theta L$ without ever fully representing either of the two Jacobians $\mathcal{J}_{\boldsymbol{x}_n}(\boldsymbol{x}_{n+1})$ and $\mathcal{J}_\theta(\boldsymbol{x}_n)$. In the reverse mode gradient accumulation, the Jacobian $\mathcal{J}_{\boldsymbol{x}_n}(\boldsymbol{x}_{n+1})$ is always transposed and then post-multiplied by the gradient vector $\nabla_{\boldsymbol{x}_{n+1}} L$. Using the above formula for the Jacobian, this product is

$$\begin{aligned}[\mathcal{J}_{\boldsymbol{x}_n}(\boldsymbol{x}_{n+1})]^\mathsf{T}\nabla_{\boldsymbol{x}_{n+1}} L &= [\boldsymbol{I} + u_2\boldsymbol{d}\nabla_{\boldsymbol{x}_n}[\alpha^+]^\mathsf{T} + (1-u_2)\boldsymbol{d}\nabla_{\boldsymbol{x}_n}[\alpha^-]^\mathsf{T}]^\mathsf{T}\nabla_{\boldsymbol{x}_{n+1}} L &(17)\\ &= \nabla_{\boldsymbol{x}_{n+1}} L + u_2\nabla_{\boldsymbol{x}_n}[\alpha^+](\boldsymbol{d}^\mathsf{T}\nabla_{\boldsymbol{x}_{n+1}} L) + (1-u_2)\nabla_{\boldsymbol{x}_n}[\alpha^-](\boldsymbol{d}^\mathsf{T}\nabla_{\boldsymbol{x}_{n+1}} L). &(18)\end{aligned}$$

Computing the products right to left only involves manipulating vectors. Next, the transpose of the Jacobian $\mathcal{J}_\theta(\boldsymbol{x}_n)$ is also always post-multiplied by $[\nabla_{\boldsymbol{x}_n} L]^\mathsf{T}$ such that

$$\begin{aligned}[\mathcal{J}_\theta(\boldsymbol{x}_n)]^\mathsf{T}\nabla_{\boldsymbol{x}_n} L &= [u_2\boldsymbol{d}\nabla_\theta[\alpha^+]^\mathsf{T} + (1-u_2)\boldsymbol{d}\nabla_\theta[\alpha^-]^\mathsf{T})]^\mathsf{T}\nabla_{\boldsymbol{x}_n} L &(19)\\ &= u_2\nabla_\theta[\alpha^+](\boldsymbol{d}^\mathsf{T}\nabla_{\boldsymbol{x}_n} L) + (1-u_2)\nabla_\theta[\alpha^-](\boldsymbol{d}^\mathsf{T}\nabla_{\boldsymbol{x}_n} L). &(20)\end{aligned}$$

Appendix C. ELBO Gradient Derivation

Here we discuss optimizing the ELBO with an unnormalized energy-based model (EBM). Let the approximate posterior be given by an unnormalized density

$$q_\phi(\boldsymbol{z}) = \frac{1}{Z(\phi)} e^{f_\phi(\boldsymbol{z})}. \tag{21}$$

The reparameterized ELBO is

$$\begin{aligned}\mathcal{L}(\theta,\phi) &= \mathbb{E}_{q_\phi(\boldsymbol{z})}[\log p_\theta(\boldsymbol{x},\boldsymbol{z}) - \log q_\phi(\boldsymbol{z})] &(22)\\ &= \mathbb{E}_{p(\epsilon)}[\log p_\theta(\boldsymbol{x},\boldsymbol{z}(\phi,\epsilon)) - \log q_\phi(\boldsymbol{z}(\phi,\epsilon))] &(23)\end{aligned}$$

where $\boldsymbol{z}(\phi,\epsilon)$ is a sample generated from the slice sampler with unnormalized density $f_\phi(\boldsymbol{z})$ and the noise ϵ are the set of random variables u_1, u_2, and $\boldsymbol{d}$ used to generate the reparameterized samples. The Monte Carlo estimate of the gradient given a sample ϵ is

$$\begin{aligned}\hat{\nabla}(\epsilon,\phi) &= \nabla_\phi[\log p_\theta(\boldsymbol{x},\boldsymbol{z}(\phi,\epsilon)) - \log q_\phi(\boldsymbol{z}(\phi,\epsilon))] &(24)\\ &= \nabla_\phi[\log p_\theta(\boldsymbol{x},\boldsymbol{z}(\phi,\epsilon)) - f_\phi(\boldsymbol{z}(\phi,\epsilon)) + \log Z(\phi)]. &(25)\end{aligned}$$

This appears to require the gradient of the normalizing constant $Z(\phi)$. We can estimate this gradient using samples generated from $q_\phi(\boldsymbol{z})$ via slice sampling. However, we take a different approach. Applying the total derivative (Roeder et al., 2017), we have

$$\hat{\nabla}_{\mathrm{TD}}(\epsilon, \phi) = \nabla_{\boldsymbol{z}}[\log p_\theta(\boldsymbol{x}, \boldsymbol{z}(\phi, \epsilon)) - f_\phi(\boldsymbol{z}(\phi, \epsilon)) + \log Z(\phi)]\nabla_\phi \boldsymbol{z}(\phi, \epsilon) \tag{26}$$

$$+ \nabla_\phi[\log p_\theta(\boldsymbol{x}, \boldsymbol{z}) - \log q_\phi(\boldsymbol{z})]. \tag{27}$$

The components $\nabla_{\boldsymbol{z}} \log Z(\phi)$ and $\nabla_\phi \log p_\theta(\boldsymbol{x}, \boldsymbol{z})$ are zero. Next, we can ignore $\nabla_\phi \log q_\phi(\boldsymbol{z})$ since it has mean zero. With these terms removed, we have the path derivative estimator of the gradient that does not require the normalizing constant:

$$\hat{\nabla}_{\mathrm{PD}}(\epsilon, \phi) = \nabla_{\boldsymbol{z}}[\log p_\theta(\boldsymbol{x}, \boldsymbol{z}(\phi, \epsilon)) - f_\phi(\boldsymbol{z}(\phi, \epsilon))]\nabla_\phi \boldsymbol{z}(\phi, \epsilon). \tag{28}$$

This estimator has zero variance when $p_\theta(\boldsymbol{z} \mid \boldsymbol{x}) = q_\phi(\boldsymbol{z} \mid \boldsymbol{x})$ and favorable performance (Roeder et al., 2017). It may be surprising that we can compute low-variance gradients without the normalization constant. However, inspection of the pathwise gradient tells we can do just that since the path through $\boldsymbol{z}$ via slice sampling does not depend on the normalization constant.

Unfortunately, evaluation of the full ELBO *does* require the normalization constant of the approximate posterior, which is no longer available.

Appendix D. Additional experiment

We implemented the simulated inference network example from Rainforth et al. (2018), Section 4. In this example the generative model is

$$\boldsymbol{z} \sim \mathcal{N}(\mu, I), \quad \boldsymbol{x} \mid \boldsymbol{z} \sim \mathcal{N}(\boldsymbol{z}, I) \tag{29}$$

where $\boldsymbol{x} \in \mathbb{R}^D$ are the observations and $\boldsymbol{z} \in \mathbb{R}^D$ are the latent variables. We fit the model by optimizing the ELBO with approximate posterior $q(\boldsymbol{z} \mid \boldsymbol{z}) = \mathcal{N}(A\boldsymbol{x}+b, \frac{2}{3}I)$. The parameters are the generative parameters $\mu \in \mathbb{R}^D$ and the inference network parameters $A \in \mathbb{R}^{D\times D}$ and $b \in \mathbb{R}^D$. For a dataset $\{\boldsymbol{x}\}_{1:N}$, the optimal parameters (Rainforth et al., 2018) are

$$\mu^* = \frac{1}{N}\sum_{i=1}^{N} \boldsymbol{x}_i, \quad A^* = I/2, \quad b^* = \mu^*/2. \tag{30}$$

We simulated $N = 1000$ samples from this model and fit the generative and inference network parameters using slice sampling reparameterization gradients. The dimensionality was $D = 20$, the mini-batch size as 128, and we computed the slice sampling gradient using $S = 20$ samples after a 30 sample burn in. All parameters (true and fit) were initialized from standard multivariate Gaussian distributions. After optimizing for 1000 iterations, the fit parameters were very close to the optimal values (Figure 5).

Appendix E. Implementation details

As mentioned in the main text, we implemented the forward slice sampling with numerical root finding and reverse mode automatic differentiation in JAX Bradbury et al. (2018). Here we describe three primary components of our implementation.

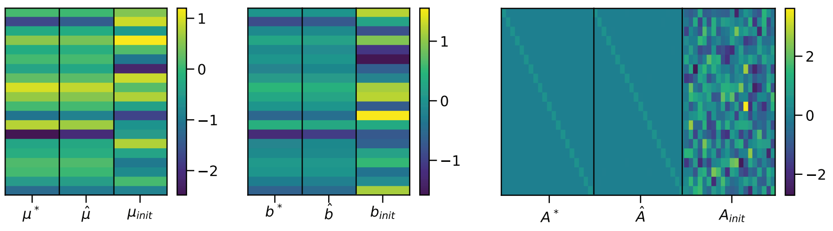

Figure 5: True ($*$), fit ($\hat{}$), and initialized (*init*) parameters from the simulated inference network experiment (Rainforth et al., 2018).

Root finding The forward sampling process for the reparameterized slice sampling algorithm requires numerical root finding to identify the slice endpoints. This corresponds to finding the α^+ and α^- that satisfy

$$\pi(\boldsymbol{x}_n + \alpha \boldsymbol{d}; \theta) - u_1 \pi(\boldsymbol{x}_n\,; \theta) = 0. \tag{31}$$

Importantly, as mentioned above, we are interested in two specific roots: the roots $\alpha^- < 0$ and $\alpha^+ > 0$ that are closest to zero.

We used a standard bisection algorithm to identify these scalar roots. This corresponded to running two root finding operations; one bracketed below zero $\alpha^- \in [-a, \delta]$ and one bracketed above zero $\alpha^+ \in [\delta, a]$ where δ is a small positive constant. Notably, for multimodal distributions there may be multiple roots inside the brackets, and the bisection algorithm will only be guaranteed to find one of these roots (rather than the root closest to zero). Therefore we first identified the bracket value a with a stepping out procedure. We did this by stepping out a logarithmically until the bracketing condition was satisfied. Once the condition was satisfied, we proceeded with the bisection algorithm.

We wrote the root finder using custom code in JAX such that it could be compiled using `jit` and batched using `vmap`. These two features are critical for speed. The `jit` compilation makes the root finding fast, and `vmap` makes it easy and fast to batch the root finding operation across multiple independent sampling chains.

Forward sampling The forwards sampling process takes as input random noise variables, the current parameters, and a function that computes the log probability of the distribution of interest (up to an additive constant). It proceeds with the slice sampling steps, using the root finding implementation described in the previous subsection to identify the roots. We also implemented this function to be compiled using `jit` and batched across multiple chains using `vmap`.

Reverse mode gradients We implemented the backwards pass using the efficient computations described in B. Again, we implemented this function to be compiled using `jit` and batched across multiple chains using `vmap`.